

All-Optical Loadable and Erasable Storage Buffer Based on Parametric Nonlinearity in Fiber

Anjali Agarwal, *Member, IEEE, Member, OSA*, Lijun Wang, Yikai Su, and Prem Kumar, *Fellow, IEEE, Fellow, OSA*

Abstract—We present a loadable and erasable all-optical fiber storage buffer based on parametric gain and cross-phase modulation (XPM) loading. The gain is provided by a phase-sensitive amplifier (PSA), implemented as a Sagnac interferometer, and relies on the nonlinear interaction within standard dispersion-shifted fiber. PSAs inherently have the property of stabilizing *ones* and *zeros* and thus eliminate the need to use optical filters within the buffer, or the need for any other kind of intensity discriminator. The action of the PSA is then twofold. It provides the gain and also achieves bistability of the buffer, which gives it an advantage over a linear amplifier such as erbium-doped fiber amplifier for our experimental configuration. External data are written into the buffer using wavelength-induced XPM. This method is insensitive to the optical phase of the incoming data and thus does not require tracking of its phase. The buffer is erased by employing a nonlinear optical loop mirror as a switch. We demonstrate storage of picosecond pulse packets at bit rates of 1 Gb/s for periods of time up to 1 ms.

Index Terms—Fiber optic communications, fibers, nonlinear optics.

I. INTRODUCTION

REALIZATION of high-speed optical networks would rely on some key enabling technologies, some of which include high-speed optical sources, optical switches, clock recovery, wavelength converters, and optical buffers [1]. Buffering can provide for contention resolution. At the receiver, optical buffers are employed when the receiver is incapable of processing data fast enough. Optical buffers accept and store packets at the full bit rate, while the receiver reads it out at a slower rate. Buffers are also useful in storing the high-rate data, while its rate is converted to interface with low-speed electronics. An optical buffer is critical for low packet-loss probability in future photonic packet-switched networks. In particular, they would be required to store packets during rate conversion and header

processing, and to overcome the receiver bottleneck. They would be required for queuing packets while transmitters await access to the network. In general, optical buffers are essential to provide the increased functionality needed to implement networking functions and provide the ability to manipulate bit streams at ultrahigh bit rates [2], [3].

Two requirements of an optical buffer are preservation of timing of pulses and bistability, i.e., simultaneous stability for both *ones* and *zeros* [4], [5]. Several types of optical buffers have been demonstrated based on recirculating or regenerative fiber loops. Recirculating storage buffers have conventionally been realized using erbium-doped fiber amplifiers (EDFAs) as the gain element and require amplitude modulation using either an electro-optic modulator or a cross-gain saturation in a semiconductor optical amplifier to provide timing stability [6]–[8]. In addition, a filter is required to reject the amplified spontaneous emission (ASE) and thus prevents the noise from building up in the *zero* time slots. Storage has been demonstrated up to rates of 40 Gb/s [6]. Here the speed of the modulator limits the speed of the optical buffer. Regenerative storage rings availing fiber-optic gates have achieved storage up to rates of 1 Gb/s [9]–[11], and also at 40 [12] and 20 Gb/s [13] by using an ultrafast nonlinear interferometer [14]. A totally different approach to the buffer design makes use of parametric amplification to nullify the round-trip linear loss within the storage buffer.

Previously, we have demonstrated buffers employing phase-sensitive [15], [16] and phase-insensitive [18] parametric amplification to compensate the round-trip loss in the buffer. Phase-sensitive amplifiers (PSAs) are self-stabilizing and have been shown to exhibit several useful properties such as near 0 dB noise figure and low soliton timing jitter. These two properties control the noise within the cavity and thus ensure that the pulse does not stray from its proper timing and that *zeros* remain *zeros*. One can exploit these useful properties of PSAs to implement buffers without having to use modulators or filters [19], [20], which simplify their design considerably. Thus, PSAs not only provide gain within the buffer but also have pulse shaping and noise reduction properties that help mitigate signal deterioration. This is the motivation to design an all-optical storage device that utilizes PSAs. The PSA is implemented as a nonlinear fiber Sagnac interferometer (NFSI) [21]. This configuration helps to conveniently separate the pump and the stored signal.

Earlier, we reported experimental results on storage [17]. In this paper, we elaborate on the principles and performance of

Manuscript received January 11, 2005; revised March 29, 2005. This work was supported in part by the Defense Advanced Research Projects Agency, through the AFOSR, under Grant F49620-96-1-0262. This paper is based on preliminary accounts presented at Optical Fiber Communication Conference 2000 and Optical Fiber Communication Conference 2001.

A. Agarwal is with Telcordia Technologies, Red Bank, NJ 07701 USA (e-mail: anjali@research.telcordia.com).

L. Wang is with China Broadband Communications Inc., Beijing, China (e-mail: Lijun.wang@126.com).

Y. Su is with Shanghai Jiao Tong University, Shanghai 200030, China (e-mail: yikaisu@sjtu.edu.cn).

P. Kumar is with the Center for Photonic Communication and Computing, Department of Electrical and Computer Engineering, Northwestern University, Evanston, IL 60208-3118 USA (e-mail: kumarp@northwestern.edu).

Digital Object Identifier 10.1109/JLT.2005.850025

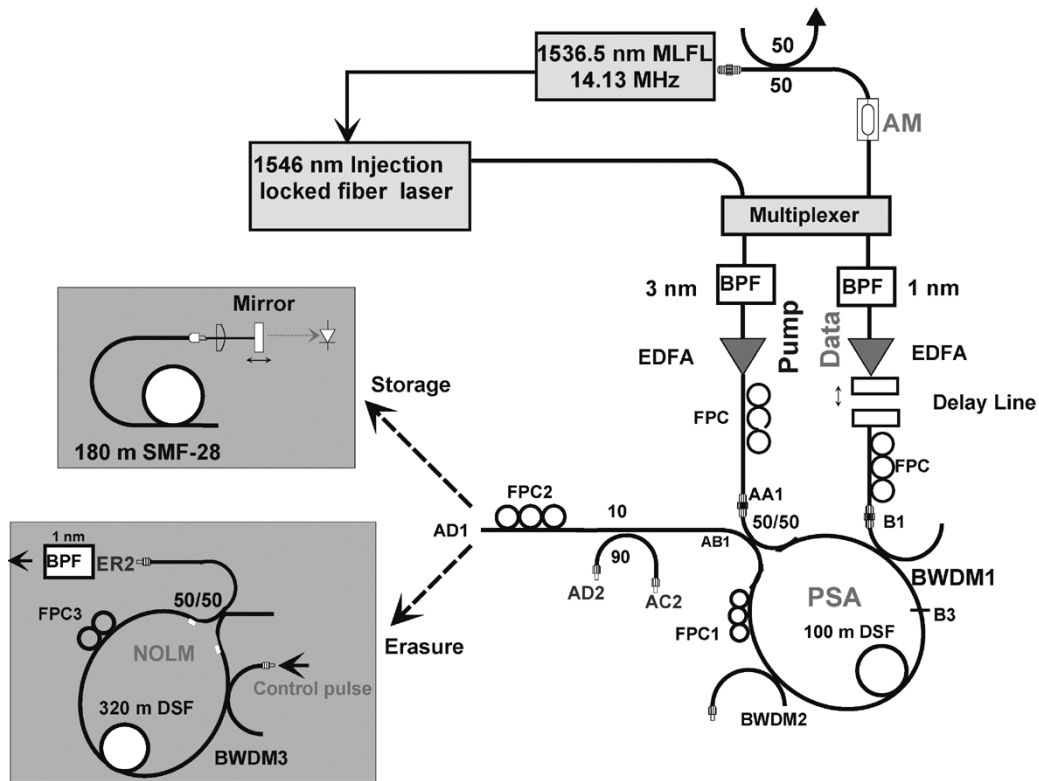


Fig. 1. Experimental configuration of the 32-b storage buffer utilizing XPM loading and phase-sensitive amplification. AM: amplitude modulator; EDFA: erbium-doped fiber amplifier; FPC: fiber polarization controller; PSA: phase-sensitive amplifier; DSF: dispersion-shifted fiber; SMF-28: single-mode fiber; BWDM: bandpass wavelength division multiplexer.

this buffer. In an all-optical communication network, data are required to be “written” or “loaded” into the buffer optically. In this paper, loading of externally generated data packets by phase-insensitive wavelength-induced cross-phase modulation (XPM) within a Sagnac interferometer PSA is described [16]. This method of loading eliminates the need to match the phase of the incoming data to that of the local pump. In the absence of XPM, the Sagnac interferometer behaves like a mirror. Through XPM, the data pulses introduce a relative phase shift between counter-propagating pump pulses inside a Sagnac interferometer PSA. This switches or loads a copy of the externally generated data pulses at the pump wavelength into the storage buffer. Once externally generated data have been optically loaded and stored within the fiber buffer, it might be required to be “unloaded” or “erased” (in order to load and store new data). This is also implemented optically here. A nonlinear optical loop mirror (NOLM) is used as an optical switch within the buffer. During storage, the NOLM acts as a mirror, while during erasure of the buffer, it acts as a switch and switches the stored data out of the buffer. The buffer is erased once the stored data are switched out of the buffer [17].

II. EXPERIMENTAL CONFIGURATION

The experimental system is shown in Fig. 1. Implementation of wavelength-induced XPM requires synchronized sources

at different wavelengths. In our system, two passively mode-locked Er:Yb-doped fiber lasers using loss modulation in a fast saturable absorber (SA) are used. The master laser is a linear cavity laser and is used to injection lock a similar fiber laser once the optical paths of the two cavities have been matched. Both lasers have a fundamental repetition rate of 14.13 MHz and are tunable in wavelength. The master laser has an average output power of 1.5 mW (21 W peak power) and its wavelength is tuned to 1536.5 nm. It produces 5-ps (full-width at half-maximum) transform-limited pulses. The slave laser generates 7-ps pulses, has an average output power of 0.5 mW (5 W peak power), and its wavelength is set to 1546 nm.

The output pulses from the master laser at a wavelength of 1536.5 nm are modulated using an electro-optic amplitude modulator (AM). The AM is driven by a pattern-generating timing circuit that is synchronized to the master laser output. The bit rate is 14.13 Mb/s at this point. The modulator generates 32-b binary data packets consisting of eight *ones* followed by 24 *zeros*. It is worth noting that the choice of eight successive *ones* followed by 24 *zeros* was completely arbitrary and was prompted by our method of using a slow photodiode to observe long-term storage. The output of the modulator is amplified to an average power of 1 mW. Now the pump pulses and data packets are both inputted to an optical multiplexer. The optical multiplexer is used to scale the bit rate from 14 Mb/s to 1 Gb/s. It consists of 50/50 couplers with a fixed delay incorporated between the two output ports of the couplers to generate

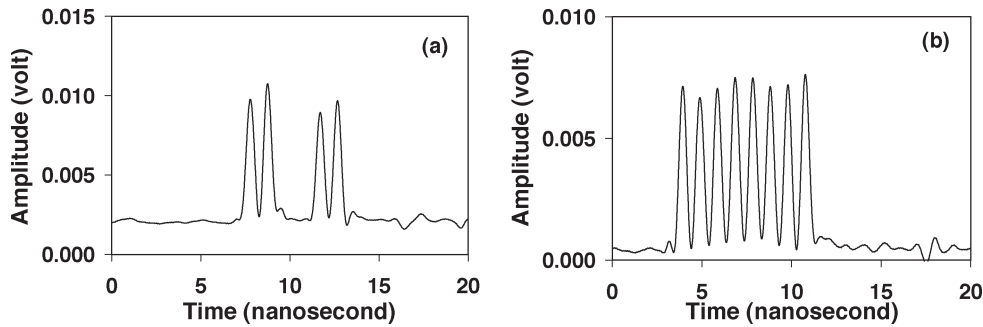


Fig. 2. (a) 1 Gb/s data packet and (b) pump pattern produced by the optical multiplexer.

1 Gb/s data and pump pulses. The data pattern at a wavelength of 1536.5 nm and at a bit rate of 1 Gb/s consists of 11001100 with each bit separated by 1 ns. The corresponding pump at a bit rate of 1 Gb/s will have to be all *ones* and thus consists of 11111111. The data and the corresponding pump pattern are shown in Fig. 2. Fiber polarization controllers (FPCs) are also used at appropriate positions to ensure that all the pulses in the pump and data pattern have the same polarization. In order to observe storage, it is critical to have all pump pulses in the 1 Gb/s pulse stream of the same polarization. Once the bit rate of both pump and data is increased to 1 Gb/s, fiber-coupled optical bandpass filters are used in each arm to select the wavelength. Thus, the pump is set to a wavelength of 1546 nm and the data are set to a wavelength of 1536.5 nm.

In this way, the data packet is modulated by an AM and an optical multiplexer. The AM is used to turn ON eight (or one, depending on the configuration of the timing circuit to the modulator) data packets and then block the next 504 (or 63) packets. Each data packet consists of 32 B of information of which 8 B is ON and 24 B OFF. Each byte of information is modulated by the optical multiplexer and consists of the data pattern 11001100 at a bit rate of 1 Gb/s. Hence, data are presented to the buffer eight (or one) times (for loading) and then switched OFF for 1.14 ms (or 140 μ s), during which storage occurs.

The pump pulses at a wavelength of 1546 nm are now amplified to an average power of 25 mW (30 W peak power), while the data pulses are amplified to an average power of 0.7 mW (1.75 W peak power). FPCs are used in both pump and data arms to align the polarizations optimally for XPM switching. For a very effective nonlinear interaction in the dispersion-shifted fiber (DSF) fiber within the NFSI, the pump and data pulses must exactly overlap. This requires fine adjustment of the optical paths of pump and data arms and is achieved by means of a tunable delay line placed in the data arm.

The PSA that was configured as an NFSI consists of a 3-dB coupler whose output ports are spliced to a 100-m length of standard DSF with a zero-dispersion wavelength (λ_0) of 1537 nm. An FPC within the interferometer is required to bias it as a perfect reflector for pump pulses in the absence of data pulses. The PSA also consists of two bandpass wavelength division multiplexers (BWDMs) that are wavelength selective couplers. The first BWDM is used to multiplex the

pump and data pulses, whereas the second BWDM placed after the dispersion-shifted fiber is used to couple the data pulses (1536.5 nm) out of the PSA, while transmitting the pump pulses (1546 nm). The pump pulses are injected at one input port AA1 of the 3-dB coupler. The second input port AB1 is connected to a 10/90 coupler and a fiber polarization controller. The storage line is terminated either in an end-mirror (for the storage experiments) or in a NOLM (for the erasure experiments). The end-mirror has a transmission of 15% and is placed on a translation stage in order to adjust the length of the storage buffer (formed by the storage line and the PSA) to accommodate exactly 32 B of data (or one packet). This ensures that the stored pulses (in a byte) after every round-trip overlapped with the corresponding pump pulses (in a byte) in the PSA and were then amplified. The storage buffer has a round-trip length of approximately 453 m, which is the length required to store 32 B. The NOLM is formed with a 50/50 coupler, whose output ports are spliced to 320 m of DSF with a zero-dispersion wavelength (λ_0) of 1538 nm. Also included in this loop is an FPC to bias the NOLM as a perfect reflector in the absence of a control pulse. The NOLM will be described later in greater detail in the section describing erasure of the buffer. Once the data are loaded into the storage line, it can be maintained as long as the loss of the fiber buffer (PSA + storage line) is equalized by the gain of the PSA. As the switched signal propagates in the storage line, it undergoes both linear and nonlinear phase shifts. If the relative phases of this returning signal pulse and the pulse used to pump the PSA are optimum for amplification by the PSA, the signal is amplified sufficiently to overcome the round-trip loss of the buffer and is thus stored.

III. PSA GAIN

We first tested the PSA by disconnecting the storage line at AD1 (see Fig. 1). The output of a passively mode-locked fiber laser is split and amplified to generate the pump and data pulse streams, with FPCs to control their polarization. The pump is connected to one input port AA1 of the PSA and the data are injected into the PSA via the 10% port AD2 of the 10/90 coupler, which is connected to the second input port of the PSA. For this experiment, the radio frequency (RF) drive to the modulator is turned off and the multiplexer is also removed. The PSA that was configured as a Sagnac interferometer works

as a reflector in the absence of data pulses. The pump leakage at port AD1 is 0.03% and can be neglected. The pump and data paths are matched and their polarization is optimally aligned. The amplified signal, observed at AD1, slowly varies through a maximum and a minimum corresponding to amplification and deamplification according to (1), which is the PSA gain derived for continuous wave (CW) excitation [22].

$$G_s = \cos^2(\Delta\theta) + \frac{P_o}{S_o} \sin^2(\Delta\theta) + \sqrt{\frac{P_o}{S_o}} \cos(\delta) \sin(2\Delta\theta) \quad (1)$$

where the nonlinear phase shift is

$$\Delta\theta = \gamma L \sqrt{P_o S_o} \sin(\delta) \quad (2)$$

$\gamma = 2\pi n_2 / \lambda A_{\text{eff}}$, and δ is the initial phase difference between the pump and the data. Maximum gain occurs for $\sin(\delta) = 1$ and defines the signal gain quadrature. The amplification and deamplification of the signal occur due to a phase drift between the data and the pump, resulting from random variations in the path length along the pump and data arms. To find the gain of the PSA (neglecting losses), the reflected signal at port AD1 in the absence of pump pulses is compared to the amplified signal at port AD1 in the presence of pump pulses.

By alternately varying the pump and data average powers, the gain of the PSA is characterized. Fig. 3 shows the gain as a function of peak pump power for various input data powers. The lines represent the theoretical gain according to (1) for average data powers of 41 μW (solid line) and 150 μW (dashed line). The solid points represent the experimental gain data obtained from the PSA for average data powers of 41 μW (solid circle) and 150 μW (solid triangle). Values of various parameters used here are n_2 (fiber nonlinearity) = $3.2 \times 10^{-20} \text{ m}^2/\text{W}$, $\lambda = 1.55 \mu\text{m}$, A_{eff} (effective area of fiber mode) = $6.3 \times 10^{-11} \text{ m}^2$, and L (length of fiber) = 53 m. $P_o(S_o)$ is the peak power of pump (data) pulses. As seen in Fig. 3, mostly there is good agreement between the theoretical and the experimental gains. It must be noted that the experimental data plotted here are for a pulsed pump. Hence, the signal gain is slightly different from that predicted by the CW theory used to derive (1).

IV. XPM SWITCHING

XPM is employed to load the external data into the storage buffer in a phase-insensitive manner. Using XPM, it is possible to switch the power of the pump pulses in the NFSI to the storage line. The NFSI is based on the relative phase shift between two counter-propagating pulses caused by a control pulse (data pulses in this case). In the absence of data (*zero* pulse), the interferometer is a perfect mirror and the entire pump is reflected back without any being switched (i.e., a *zero* is switched). With data injected (*one* pulse) at a different wavelength from the pump, there is a phase imbalance due to XPM and the interferometer is no longer a perfect mirror. Thus, some part of the pump is switched over (i.e., a *one* is switched). Hence, the NFSI copies the data pattern onto the pump wavelength and switches it into the fiber storage

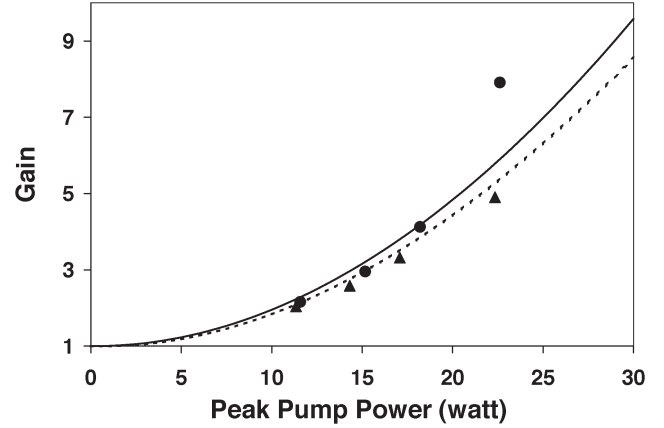


Fig. 3. Measured PSA gain (symbols) as a function of peak pump power for 41 μW (solid circle) and 150 μW (solid triangle) of average input data power. Dashed and solid lines are theoretical fits.

line. Once the data pattern is written into the buffer, it needs to be amplified by the PSA in order to be stored. Next we measure the switched pump power for various values of data power and compare the experimentally observed results with the theoretical values, which are obtained from the following equation:

$$P_1^x = P_0^x \sin^2 \left(\frac{\phi_2^x}{2} \right) \quad (3)$$

where P_0^x is the peak input pump power in \hat{x} polarization and P_1^x is the peak switched pump power in \hat{x} polarization.

$$\phi_2^x = \gamma L [2P_s^x] \quad (4)$$

where $\gamma = 2\pi n_2 / \lambda A_{\text{eff}}$, L is the length of fiber, and P_s^x is the peak data power in \hat{x} polarization. The ratio of switched pump to input pump power is given by

$$\frac{P_1^x}{P_0^x} = \sin^2 \left(\frac{\phi_2^x}{2} \right). \quad (5)$$

To measure the percentage of switched pump power, the storage line is disconnected at AD1. The pump (1546 nm) is input at AA1 and the data (1536.5 nm) are introduced into the NFSI through BWDM1 at port B1. For this experiment, the RF drive to the modulator is turned off. The pump and data arms are path matched and their polarization is optimally aligned. The NFSI works as a reflector in the absence of data and hence the pump is entirely reflected back. The pump leakage at port AD1 is negligible. The data power is varied and the switched pump power is measured at port AD1.

Fig. 4 shows the percentage of switched pump power as a function of the peak data power. The solid triangles represent the experimentally observed values, while the line is the theoretical curve obtained from (5). Values of various parameters used here are $n_2 = 3.2 \times 10^{-20} \text{ m}^2/\text{W}$, $\lambda = 1.55 \mu\text{m}$, $A_{\text{eff}} = 6.3 \times 10^{-11} \text{ m}^2$, and $L = 100 \text{ m}$. As seen in Fig. 4, mostly there is good agreement between the theoretical and the experimental

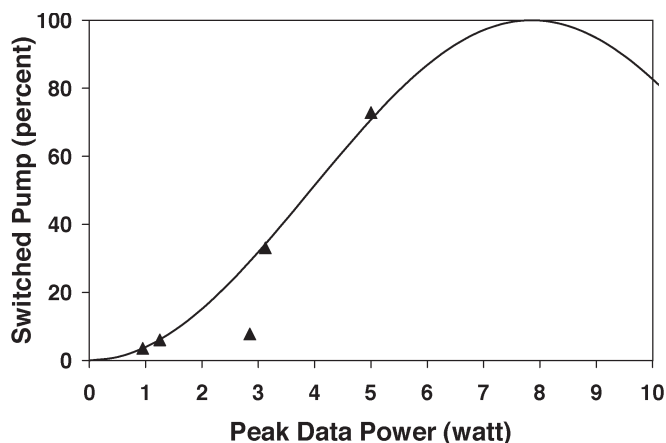


Fig. 4. Experimentally measured switched pump (triangle) as a function of peak pump power. The solid line is a theoretical fit.

values. The data point at a peak power of approximately 3 W does not fit very well to the theoretical curve. In this case, it is likely that the system was not optimized in terms of path matching and polarization.

V. STORAGE EXPERIMENTS

To demonstrate storage of the 1 Gb/s data pattern, the NFSI is set to be maximally reflecting for pump pulses in the absence of data pulses. Thus the pump leakage is minimized at AD2 by adjusting FPC1. The pump pulses are amplified to an average power of 25 mW (30 W peak power), while the data pulses are amplified to an average power of 0.7 mW. Then the pump and data arms are path matched so that the two pulses overlap within the interferometer after BWDM1 at B3. Finally, their polarizations are adjusted to observe maximum switching at a pump wavelength of 1546 nm at port AD2. The storage line comprising of 170 m of the SMF-28 fiber and a movable end-mirror is connected to port AD1. The positions of the end-mirror and FPC2 within the storage line are adjusted to get oscillations of the pump leakage. Once these oscillations are observed, it can be concluded that the optical path length of the buffer is an integral multiple of the optical path length of the laser sources. In this case, the buffer length is 32 times that of the laser cavity length. It is critical to adjust the buffer cavity length in order to ensure that the stored signal byte reflected from the end-mirror towards the PSA overlaps exactly with a byte of pump pulses injected at AA1. FPC2 is adjusted optimally to ensure that the returning pulse has the correct phase and polarization in order to be amplified by the PSA. In other words, oscillations of the pump leakage indicate that the gain of the PSA is sufficient to overcome the round-trip loss of the buffer. The round-trip loss of the buffer (PSA and storage line) is 10 dB. Once a copy of the data pattern is loaded, it is amplified by the PSA and hence stored. Storage requires control of the phase difference between the stored pattern and the incoming pump pulses. We did not actively stabilize this phase. From time to time this phase was optimum and storage was observed.

The contents of the storage line are monitored by means of a slow detector (100-ns response time) placed after the partially transmitting end-mirror. The slow detector is used to monitor the long-term storage within the buffer. The output of the photodetector is recorded on a 200-MHz digital sampling scope (Lecroy 9304A). In order to check maintenance of the 1 Gb/s data pattern, a fast detector with a bandwidth greater than 1 GHz is employed. The output of this fast photodiode is recorded on a real-time sampling scope with a sampling rate of 4 GSamples/s (HP54720A). Hence, in order to check the reliability of the stored data packets, two photodiodes are required: a slow one for checking the total storage time, and a fast photodiode to ensure maintenance of *ones* and *zeros* in the 1 Gb/s B of data.

Fig. 5 illustrates the storage results obtained for a 1 Gb/s data pattern loaded in the buffer through XPM and stored using phase-sensitive amplification. In this figure, the three traces show the long-term storage results observed with the slow photodiode connected to the 200-MHz digital sampling scope. As is evident in these traces, each individual packet is not visible. Instead, each individual packet is seen represented by a peak. Storage is observed for 1 ms as shown by the three traces in Fig. 5. Initially, the eight XPM-loading events are seen followed by storage of these loaded packets for approximately 450 circulations within the buffer. The structure seen during the initial eight XPM-loading events can be explained by PSA gain saturation and is due to injected data packets. Each of these eight loaded packets (except the first one) consists of two packets: the injected data packet, and the stored packet after one round-trip. These two packets have similar phases because they add constructively. Hence, the loaded packets are seen to have gradually increasing amplitudes. Once the optical power within the buffer is sufficient to saturate the PSA, the gain is lower than the total buffer loss. When the power in the storage line is low enough and the PSA is no longer saturated, the PSA gain equals the buffer loss. Then the stored packets settle to a stable amplitude. Stored packets are seen for the next 450 round-trips.

Fig. 6 shows an expanded view of the stored packets. These traces display the response of the slow photodiode clearly. The slow photodiode cannot respond to each individual pulse in the byte of data. Hence, each byte is seen represented as a spike in Fig. 5. The slow photodiode charges for every byte that is ON, but is unable to discharge completely between successive bytes. The eight spikes thus correspond to the 8 B that is ON. After these 8 B, the photodiode discharges slowly as the next 24 B that is OFF arrives, until the next packet of 8 B ON and 24 B OFF arrive, where it then begins to charge again. Fig. 6(a) shows the stored packets after 320 μ s, while Fig. 6(b) shows the stored packets sometime in the middle of the storage time, after 630 μ s. Fig. 6(c) shows the stored packets towards the end of the storage time at 975 μ s. It is apparent that the 32-B packet is maintained.

It is now left to see that the 1 Gb/s data pattern generated by the optical multiplexer placed after the AM is also preserved. For this, the contents of the storage buffer are monitored with

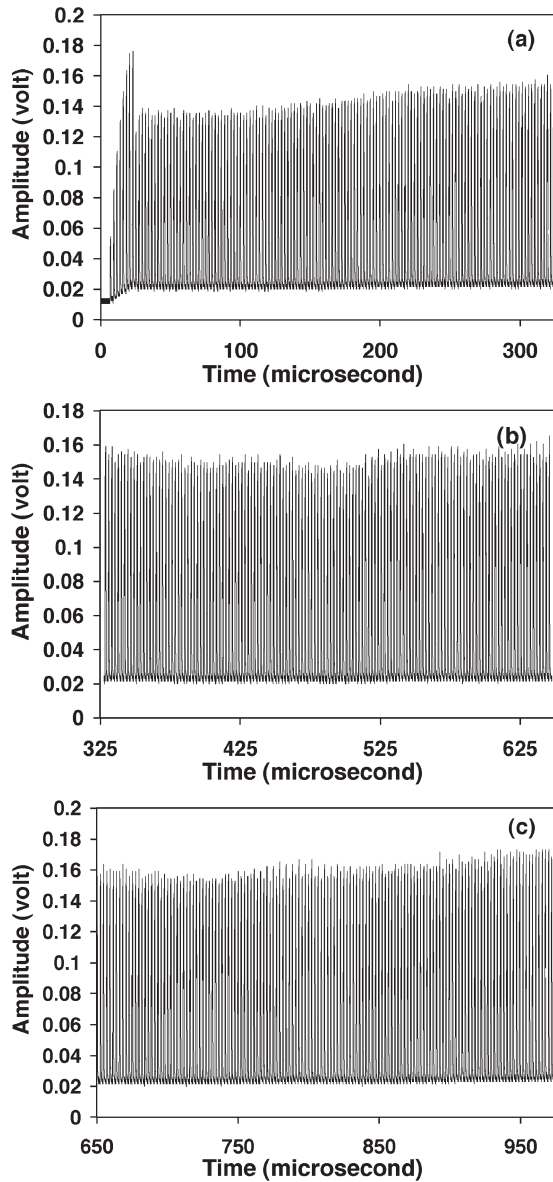


Fig. 5. Long-term storage of data at 1 Gb/s within the buffer observed using a slow photodiode. Storage is observed for 1 ms. (a) 0–325 μ s. (b) 325–650 μ s. (c) 650–975 μ s.

a fast photodiode connected to a fast real-time sampling scope. This is illustrated in Fig. 7.

The 1 Gb/s data pattern is shown after a delay of 250, 400, and 600 μ s in the three traces in Fig. 7. As is evident, the data pattern 11001100 is maintained without any apparent degradation in the extinction ratio for ones and zeros. Thus, ones remain ones and zeros remain zeros.

We strived to have all pulses in the pump pulse stream to be of the same polarization. Nevertheless, the pump pulses did not have exactly the same polarization, owing to the experimental difficulty of setting various FPCs, and hence the corresponding stored signal pulses do not see the same gain. This could be one reason that the pulses in the stored byte (shown in Fig. 7) do not have the same amplitude. Nevertheless, the

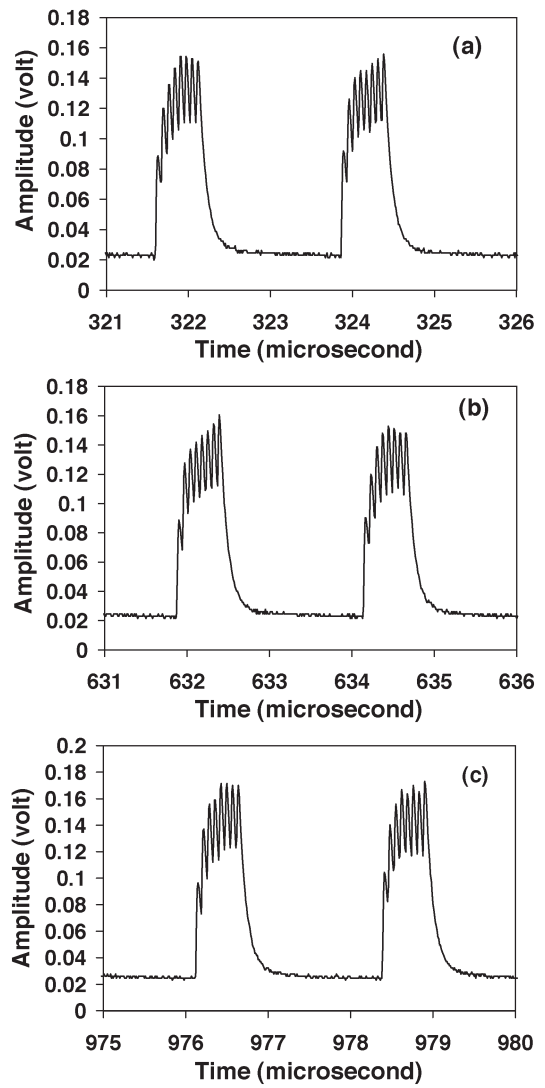


Fig. 6. Expanded view of the stored packets within the buffer. (a) After 320 μ s. (b) After 630 μ s. (c) After 975 μ s.

fact that the different pulses in the stored byte stabilize at a different peak power is an important experimental observation. Further theoretical work is needed to understand this behavior, as this is not predicted by the previous theoretical studies [19], [23], [24].

The above data show storage for 1 ms, corresponding to almost 450 circulations within the buffer. It was not possible to record storage for a duration longer than 1 ms because the sampling scope used to record long-term storage did not have sufficient memory depth to go to longer time scales. Nevertheless, we expect milliseconds to be the typical storage time for a buffer employing phase-sensitive amplification. If the phase of this buffer is stabilized, then the storage times could be much higher.

It should be noted that it is not necessary to present the external data packets eight times to the buffer. This was done here as the timing circuit to the AM was configured in this manner. Single-shot loading can be achieved if the external

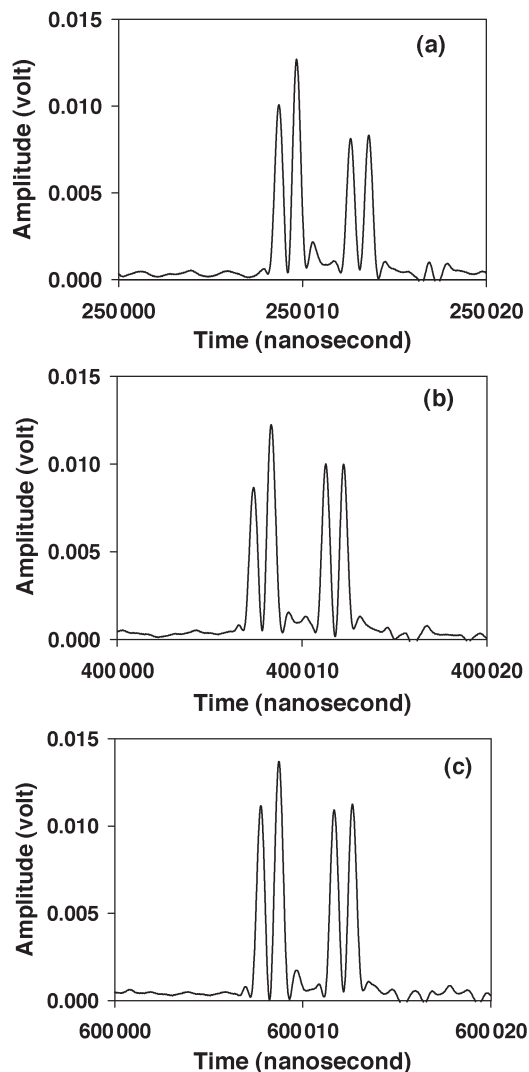


Fig. 7. Close-up view of the 1 Gb/s stored bytes within the buffer. (a) After 250 μ s. (b) After 400 μ s. (c) After 600 μ s.

data packet has sufficient power to initiate storage and was also observed in our experiments.

A. *Inverted Storage*

Besides the storage results presented in the previous section, there were other unexpected observations while performing the experiments, one of which is the occurrence of “inverted storage.” We did not extensively investigate this, but discuss it briefly here.

The storage line was optimized and the pump and data arms were path matched in order to observe loading of the external data packets. Long-term storage was monitored by a slow photodiode (100-ns response time) placed after the partially transmitting end-mirror. The photodiode was connected to a 200-MHz digital sampling scope. Fig. 8 illustrates the results obtained. Fig. 8(a) shows the eight XPM-loaded packets followed by the “inverted storage” for 200 μ s. Fig. 8(b) and (c) shows expanded views of the stored packets after 65 μ s and

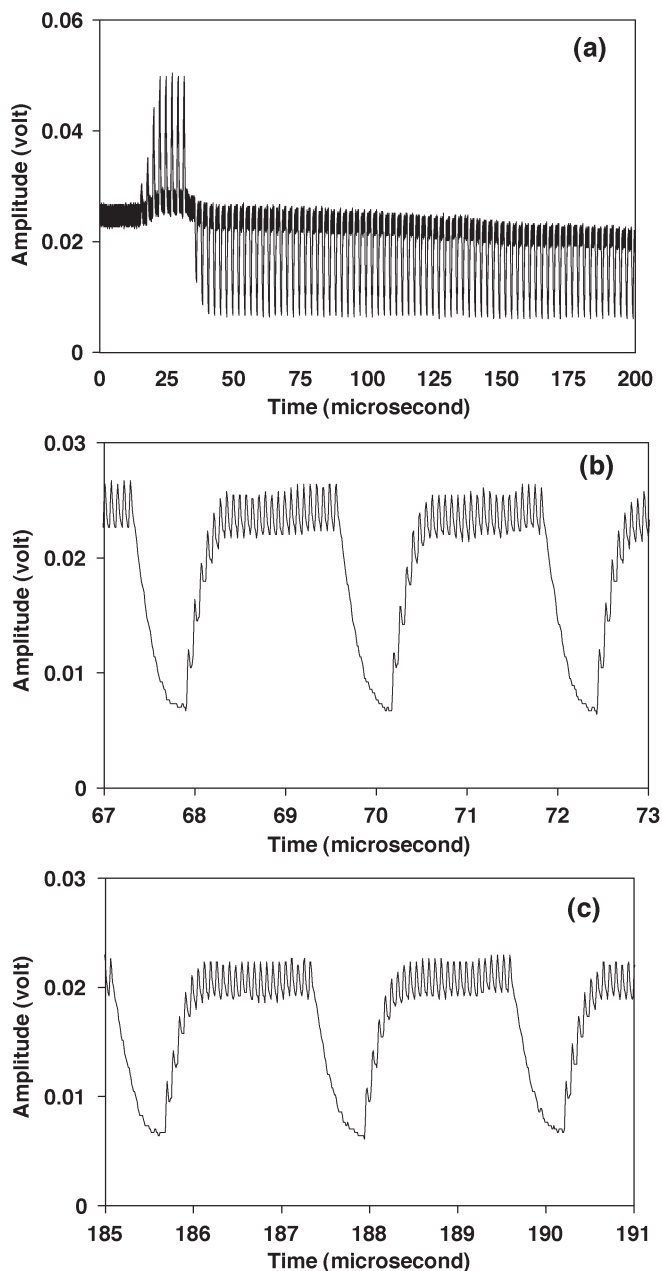


Fig. 8. Output of the storage buffer illustrating an “inverted storage.” (a) Inverted storage observed for 200 μ s. (b) Expanded view of the stored packets within the buffer after 65 μ s and (c) after 185 μ s.

after 185 μ s, respectively. The response of the slow photodiode to the 32-B data packet consisting of 8 B ON and 24 B OFF is clearly seen, but is inverted. The photodiode cannot respond to each individual pulse in the 1 Gb/s data byte. Hence, each byte is seen represented as a spike.

It appears that there is a π phase shift between the loaded and the stored packets. We are not sure about the reason for this odd observance. One possibility is that the storage buffer is oscillating when the loading packet arrives, with the phase of the pulses such that the *ones* are erased. Such a scenario is possible because the cavity phase was not stabilized, and would

explain the observations. A detailed study through experiments and simulations would be required to provide an insight into this behavior of the storage buffer.

VI. ERASURE EXPERIMENTS

To demonstrate erasure of the buffer, port AD1 is connected to the NOLM (cf. Fig. 1). A wavelength selective coupler BWDM3 within the NOLM is used to multiplex pulses at two wavelengths, i.e., the stored signal (1546 nm) and the control pulse (1536.5 nm). It is a three-port device with a passband (P) in 1525- to 1543-nm range and the reflection band (R) in the 1546- to 1565-nm range. The pump pulses are amplified to an average power of 25 mW (30 W peak power), while the data pulses are amplified to an average power of 0.7 mW. When storage is desired, the NOLM works as a perfect mirror. This is achieved by means of FPC3 placed within the NOLM. The NOLM is configured as a switch when the buffer is required to be unloaded. For this purpose, a control signal is introduced in the NOLM through BWDM3 at a wavelength of 1536.5 nm. The clockwise-propagating stored pulses (1546 nm) within the NOLM see XPM due to this control signal, whereas the counter-clockwise propagating stored pulses do not undergo XPM. This leads to a differential phase shift between the two counter-propagating pulses within the NOLM. The NOLM is no longer a perfect reflector, and the stored packets are switched to port ER2 (see Fig. 1), and thus out of the buffer. With stored packets no longer directed towards the PSA, the buffer is unloaded. An optical bandpass filter set to a wavelength of 1546 nm and with a bandwidth of 1 nm is used at port ER2 of the NOLM to view the stored packets that are switched out of the buffer. The path of the control signal consists of an EDFA (to amplify to an average power of 1 mW), an FPC (to align polarization), and a tunable delay line. The control pulse and the stored signal pulse must overlap exactly within the NOLM after BWDM3. The tunable delay line helps to achieve this. The path length of the control pulse is longer by 32 B, corresponding to a fiber length of about 453 m. Hence, the control pulses meet the stored signal packet after a delay of one packet or 32 B.

The 1 Gb/s data pattern at a wavelength of 1536.5 nm is loaded into the storage line using XPM of the pump (1546 nm) by the data. Pump leakage at AD2 is minimized by adjusting FPC1 so that the NFSI is a perfect mirror in the absence of data pulses. In order to achieve maximum switching, the pump and data arms are path matched (so that they overlap within the interferometer) and their polarization is adjusted using FPCs placed in both pump and data arms. Then XPM results in the data pattern being copied into the storage line but at the pump wavelength. The length of the entire buffer (PSA + NOLM) is optimized so that a stored signal byte (1 Gb/s bit rate) returning towards the PSA overlaps exactly with the corresponding pump pulses to see maximum gain. To observe storage, the NOLM with 320 m of DSF is configured to be maximally reflecting by adjusting FPC3. Leakage is minimized at ER2 to about 2%. This high leakage is attributed to nonoptimal adjustment

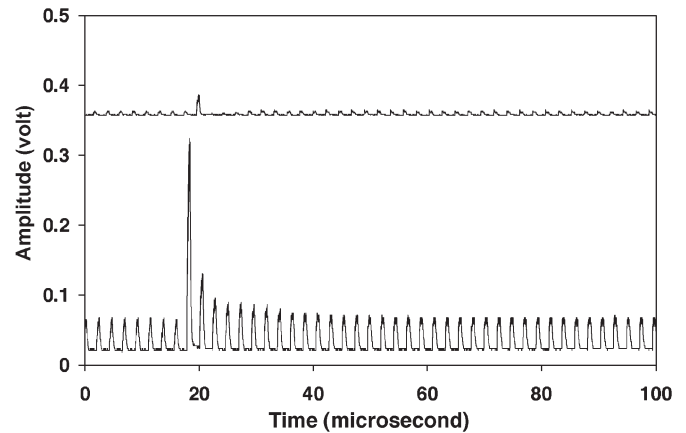


Fig. 9. Output of the storage buffer in the absence of control signal shown at port AD2 (lower trace) and port ER2 (upper trace).

of FPC3. In order to get oscillations of the pump leakage, the cavity lengths of the master and slave lasers are adjusted. Once these oscillations are observed, it can be concluded that the optical path length of the buffer is an integral multiple of the cavity length of the laser sources. In this case, it is 32 times the laser cavity length. FPC2 is also required to be adjusted to ensure that the returning stored pulses have the correct polarization and are thus amplified by the PSA. Strong oscillations of the pump leakage indicate that the buffer length is optimal and that the PSA has sufficient gain to overcome the linear round-trip loss. The contents of the buffer are monitored at ports AD2 and ER2. Port ER2 gives information of the data that are switched out of the buffer. A 1-nm optical bandpass filter centered at 1546 nm is connected to port ER2. Slow photodiodes are used and are connected to a 200-MHz digital sampling scope.

Fig. 9 depicts the output at ports AD2 (lower trace) and ER2 (upper trace). At AD2, the first XPM-loaded packet envelope is seen followed by stored packets for about 100 μ s. In this trace, each individual packet is seen as a peak only. At ER2, only a small leakage is observed because the NOLM reflects the stored packets back towards the PSA and nothing is switched out at ER2. Now, control pulses at a wavelength of 1536.5 nm are injected into the NOLM through BWDM3. Note that the loaded and stored packets are at a wavelength of 1546 nm. Fig. 10 displays the output at ports AD2 (lower trace) and ER2 (upper trace) with control pulses injected at BWDM3. It must be noted that the control pulses are injected with a delay of one packet (32 B). This allows us to see the first loaded packet at AD2 followed by a stored packet, because by this time the control pulses have yet to be injected. During this time, only a small leakage is observed at ER2. After this, the control pulses switch out the stored packets to port ER2 rather than reflecting them back towards the PSA. Hence, no more stored packets are visible at AD2. [There is seemingly another packet, but this is due to the Fresnel reflection of the injected control signal ($\lambda = 1536.5$ nm) and can be removed by an optical filter centered at a wavelength of 1546 nm.] The corresponding trace at ER2 also indicates that after the first stored packet, the next

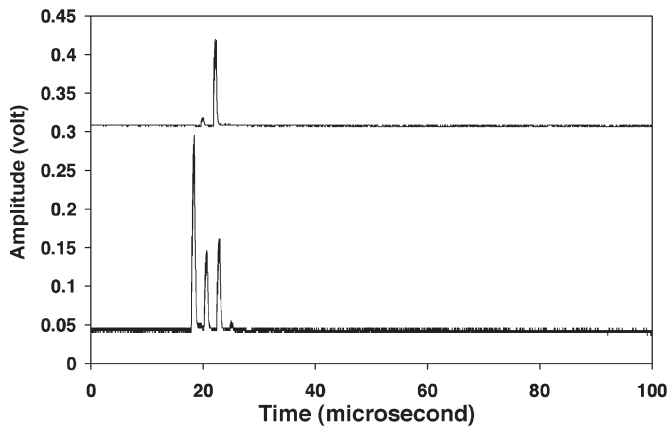


Fig. 10. Output of the storage buffer in the presence of control signal shown at port AD2 (lower trace) and port ER2 (upper trace).

stored packet is switched out and is thus visible at ER2. After this, there are no more stored packets within the buffer and hence nothing is observed either at AD2 or at ER2. Hence, the buffer contents are emptied or the buffer is erased using XPM within a NOLM.

VII. CONCLUSION

In summary, all-optical storage of picosecond pulse packets at a data rate of 1 Gb/s has been demonstrated for periods of time up to 1 ms. The storage device incorporates a PSA to offset the linear loss of the storage line. Loading of the buffer is achieved by wavelength-induced XPM. While we could not observe storage for times longer than 1 ms (due to limitations imposed by our digital sampling scope), we do not expect to see much longer storage times because environmental fluctuations are on the order of a millisecond and would thus prevent very much longer storage times. It should be noted that for most applications in an optical network, a 1-ms storage time is more than sufficient. Nevertheless, stabilization of the phase of the storage buffer should lead to an improvement in the duration of the observed storage. Speed limitation of the diagnostic instrumentation prevented from recording storage at higher bit rates. The operation of this buffer is scalable to much higher bit rates such as 40 Gb/s, which is compatible with present and future photonic networks. This is due to the fact that the inherent mechanism of this device, which is the fiber nonlinearity, is ultrafast. The response time of the nonlinear refractive index of the fiber is in the femtosecond regime. Hence, the inherent working mechanism of the buffer is not a limitation at higher data rates. High peak power, however, is an issue that has to be dealt with at high bit rates. Usage of high nonlinearity fiber (10–15 times nonlinearity of standard fiber) along with high power EDFAs would make it feasible to operate the buffer described here at data rates of 40 Gb/s.

The data are unloaded from the memory by incorporating a NOLM as an optical switch within the buffer. The mechanism of wavelength-induced XPM within the NOLM is utilized to erase the buffer. Control pulses injected in the NOLM caused

it to switch out the stored data packets from the buffer. Thus, erasure of the buffer was demonstrated.

Apart from the advantage of ultrahigh-speed operation (potentially Tb/s or greater), incorporation of a PSA provides for additional functionalities along with gain such as pulse shaping, reduced timing jitter, and noise reduction, thus mitigating signal deterioration and enhancing the stability properties of the storage ring. In other words, in our approach the PSA alone provides for gain, timing, ASE suppression, and bistability. As is the case with many other storage buffer implementations, this approach does not feature some practical functionalities such as random access buffering, variable packet lengths, and variable storage times.

REFERENCES

- [1] R. A. Barry *et al.*, "All-optical network consortium-ultrafast TDM networks," *IEEE J. Sel. Areas Commun.*, vol. 14, no. 5, pp. 999–1013, Jun. 1996.
- [2] A. Poustie, "Digital optical processing," presented at the Optical Fiber Communication Conf. 2000, OSA Technical Digest Series, Paper TuN1.
- [3] K. Hall, "High-speed TDMA techniques," presented at the Optical Fiber Communication Conf. 2000, OSA Technical Digest Series, Paper ThV4.
- [4] H. A. Haus and A. Mecozzi, "Long-term storage of a bit stream of solitons," *Opt. Lett.*, vol. 17, no. 21, pp. 1500–1502, Nov. 1992.
- [5] J. D. Moores, W. S. Wong, and H. A. Haus, "Stability and timing maintenance in soliton transmission and storage rings," *Opt. Commun.*, vol. 113, no. 1–3, pp. 153–175, Dec. 1994.
- [6] K. L. Hall and K. A. Rauschenbach, "All-optical buffering of 40-Gb/s data packets," *IEEE Photon. Technol. Lett.*, vol. 10, no. 3, pp. 442–444, Mar. 1998.
- [7] J. D. Moores, K. L. Hall, S. M. LePage, K. A. Rauschenbach, W. S. Wong, H. A. Haus and E. P. Ippen, "20-GHz optical storage loop/laser using amplitude modulation, filtering and artificial fast saturable absorption," *IEEE Photon. Technol. Lett.*, vol. 7, no. 9, pp. 1096–1098, Sep. 1995.
- [8] C. R. Doerr, W. S. Wong, H. A. Haus, and E. P. Ippen, "Additive pulse mode-locking/limiting storage ring," *Opt. Lett.*, vol. 19, no. 21, pp. 1747–1749, Nov. 1994.
- [9] V. I. Belotitskii, E. A. Kuzin, M. P. Petrov, and V. V. Spirin, "Demonstration of over 100 million round trips in recirculating fibre loop with all-optical regeneration," *Electron. Lett.*, vol. 29, no. 1, pp. 49–50, Jan. 1993.
- [10] N. A. Whitaker, Jr., M. C. Gabriel, H. Avramopoulos, and A. Huang, "All-optical, all-fiber circulating shift register with an inverter," *Opt. Lett.*, vol. 16, no. 24, pp. 1999–2001, Dec. 1991.
- [11] A. J. Poustie, K. J. Blow, and R. J. Manning, "All-optical regenerative memory for long term data storage," *Opt. Commun.*, vol. 140, no. 4–6, pp. 184–186, Feb. 1997.
- [12] K. L. Hall, J. P. Donnelly, S. H. Groves, C. I. Fennelly, R. J. Bailey, and A. Napoleone, "40-Gbit/s all-optical circulating shift register with an inverter," *Opt. Lett.*, vol. 22, no. 19, pp. 1479–1481, Oct. 1997.
- [13] M. Kalyvas, C. Bintjas, K. Zoiros, T. Houbavlis, H. Avramopoulos, L. Occhi, L. Schares, G. Guekos, S. Hansmann, and R. Dall'Ara, "All-optical write/read memory for 20-Gb/s data packets," *Electron. Lett.*, vol. 36, no. 12, pp. 1050–1052, Jun. 2000.
- [14] N. S. Patel, K. A. Rauschenbach, and K. L. Hall, "40-Gb/s demultiplexing using an ultrafast nonlinear interferometer (UNI)," *IEEE Photon. Technol. Lett.*, vol. 8, no. 12, pp. 1695–1697, Dec. 1996.
- [15] G. D. Bartolini, D. K. Serkland, P. Kumar, and W. L. Kath, "All-optical storage of a picosecond-pulse packet using parametric amplification," *IEEE Photon. Technol. Lett.*, vol. 9, no. 7, pp. 1020–1022, Jul. 1997.
- [16] A. Agarwal, L. Wang, Y. Su, and P. Kumar, "All optical storage of picosecond pulse packets using wavelength induced XPM and parametric amplification," presented at the Optical Fiber Communication Conf. 2000, OSA Technical Digest Series, Paper TuN3.
- [17] —, "All optical erasable fiber storage buffer using parametric nonlinearity in fiber," presented at the Optical Fiber Communication Conf. 2001, OSA Technical Digest Series, Paper ThH5.
- [18] L. Wang, A. Agarwal, Y. Su, and P. Kumar, "All-optical picosecond-pulse packet buffer based on four-wave mixing loading and intracavity soliton

control," *IEEE J. Quantum Electron.*, vol. 38, no. 6, pp. 614–619, Jun. 2002.

- [19] W. L. Kath, A. Mecozzi, P. Kumar, and C. G. Goedde, "Long-term storage of a soliton bit stream using phase-sensitive amplification: Effects of soliton-soliton interactions and quantum noise," *Opt. Commun.*, vol. 157, no. 1–6, pp. 310–326, Dec. 1998.
- [20] A. Mecozzi, W. Kath, P. Kumar, and C. G. Goedde, "Long-term storage of a soliton bit stream by use of phase-sensitive amplification," *Opt. Lett.*, vol. 19, no. 24, pp. 2050–2052, Dec. 1994.
- [21] G. Bartolini, R. D. Li, P. Kumar, W. Riha, and K. V. Reddy, "1.5 μm phase-sensitive amplifier for ultrahigh-speed communication," in *Optical Fiber Communication Conf., Vol. 4 of 1994, OSA Technical Digest Series*, pp. 202–203.
- [22] M. E. Marhic, C. H. Hsia, and J. M. Jeong, "Optical amplification in a nonlinear fiber interferometer," *Electron. Lett.*, vol. 27, no. 3, pp. 210–211, Jan. 1991.
- [23] J. N. Kutz, C. V. Hile, W. L. Kath, R.-D. Li, and P. Kumar, "Pulse propagation in nonlinear optical fiber lines that employ phase-sensitive parametric amplifiers," *J. Opt. Soc. Amer. B*, vol. 11, no. 10, pp. 2112–2123, Oct. 1994.
- [24] C. G. Goedde, W. L. Kath, and P. Kumar, "Controlling soliton perturbation with phase-sensitive amplification," *J. Opt. Soc. Amer. B*, vol. 14, no. 6, pp. 1371–1379, 1997.



Anjali Agarwal (M'99) received the M.S. and Ph.D. degrees in electrical engineering from Northwestern University, Evanston, IL, in 1997 and 2001, respectively.

She joined the Optical Networking Group at Lucent Technologies, Holmdel, NJ, as a Member of Technical Staff in 2001, where she made significant contributions to architecting Lucent Technologies' next-generation optical transport product. She is currently a Senior Scientist with the Optical Networking Systems group at Telcordia Technologies, Red Bank,

NJ, where she continues to provide critical innovation and research of new developments and improvements in optical communications technology. She has around 35 refereed journal and conference publications. Her current research focuses on optical code division multiple access systems.

Dr. Agarwal is a Member of Optical Society of America (OSA).



Lijun Wang received the Ph.D. degree in optical communications from the Beijing University of Posts and Telecoms, China, in 1998.

He is currently the Founder and CTO of China Broadband Communications (CBCOM), Inc., Beijing, China. Before founding and running CBCOM, he worked at Corning Incorporated, Corning, NY, as a Senior Research Scientist. Prior to joining Corning, he spent three years at Northwestern University, Evanston, IL, as a Postdoctoral Research Scientist. Since then, he has authored and coauthored of over

30 technical papers in optical fiber communications, telecommunication, and data networks. His research interests focus on Softswitch technology and next generation networks.



Yikai Su received the B.S. degree from the Hefei University of Technology, Anhui, China, in 1991, the M.S. degree from Beijing University of Aeronautics and Astronautics, China, in 1994, and the Ph.D. degree from Northwestern University, Evanston, IL, in 2001.

He was with Crawford Hill Lab of Bell Laboratories, Holmdel, NJ, for three years before he joined Shanghai Jiao Tong University, China, as a Full Professor in 2004. His research areas cover transparent optical networks, ultrahigh-speed transmission, and packet-switched networks. He has over 70 publications in prestigious international journals and conferences, including eight invited conference papers.

Prof. Su serves as a Technical Committee Member of IEEE Lasers & Electro-Optics Society'2005, ICCAS'04 and '05, and ICOCN'04, as well as a Reviewer of IEEE PHOTONICS TECHNOLOGY LETTERS, *Optics Letters*, *Optical and Laser Technology*, JOURNAL OF LIGHTWAVE TECHNOLOGY, *IEEE Proceedings—OptoElectronics*, *Optics Communications*, *Journal of Optical Networking*, and IEEE TRANSACTIONS ON CIRCUITS AND SYSTEMS II.



Prem Kumar (M'89–SM'90–F'03) received the Ph.D. degree in physics from the State University of New York, Buffalo, in 1980.

He is an SBC Professor of Information Technology in the Department of Electrical and Computer Engineering and the Director of the Center for Photonic Communication and Computing, McCormick School of Engineering and Applied Science, Northwestern University, Evanston, IL. He also holds an appointment as Professor of Physics and Astronomy in the Weinberg College of Arts and Sciences at

Northwestern University. He joined Northwestern University in 1986 after spending five years at the Massachusetts Institute of Technology, Cambridge, as a Research Scientist. He is the Founder of NuCrypt LLC, Skokie, IL, a startup company focusing on the commercialization of quantum encryption technology for securing the physical layer of fiber-optic networks. He is also an Advisory Board Member for Baird Venture Partners, Chicago, IL. During the 2000–2003 period, he served as a Scientific Advisor to Santel Networks, Newark, CA.

Dr. Kumar is a Fellow of the Optical Society of America (OSA), the American Physical Society, and the Institute of Physics. He is also a Member of the American Association for the Advancement of Science (AAAS). He currently serves as the Representative of the OSA to the Section Committee of the AAAS Section on Physics.